

Quantification of temperature-dependent CO₂ adsorption kinetics in Lewatit VP OC 1065, Purolite A110, and TIFSIX-3-Ni for direct air capture

May-Yin (Ashlyn) Low¹, David Danaci^{1,2,3}, Callum Sturman¹, Camille Petit^{1*}*

¹ Department of Chemical Engineering, Imperial College London, London SW7 2AZ, United Kingdom

²The Sargent Centre for Process Systems Engineering, Imperial College London, London SW7 2AZ, United Kingdom

³I-X Centre for AI in Science, Imperial College London, London W12 0BZ, United Kingdom

*Corresponding authors: camille.petit@imperial.ac.uk; d.danaci@imperial.ac.uk

Abstract

One of the critical factors affecting the performance of an adsorption-based direct air capture (DAC) process is the CO₂ adsorption kinetics. Yet, this data is not currently available in the literature for many DAC adsorbents, particularly at the relevant conditions for DAC (i.e. ~ 0.04%_{vol} or 400 ppm). In this study, we report temperature-dependent linear driving force constants ($k_{LDF}(T)$) measured at 400 ppm CO₂ between 20 °C and 70 °C for three promising DAC adsorbents: Lewatit VP OC 1065, Purolite A110, and TIFSIX-3-Ni. TIFSIX-3-Ni exhibits the fastest adsorption kinetics across the whole temperature range, while Purolite A110 has faster adsorption kinetics compared to Lewatit VP OC 1065 at temperatures greater than 40 °C. Overall, the $k_{LDF}(T)$ values determined in this work can be used for initial process scale modelling to assess the process performance of these adsorbents for DAC, while additional experiments would have to be conducted to determine k_{LDF} constants outside this temperature range and at different CO₂ concentrations.

1. Introduction

The abatement of anthropogenic CO₂ emissions is no longer considered sufficient to achieve climate change mitigation targets. Removal of historical CO₂ emissions from the atmosphere is now necessary [1], and adsorption-based direct air capture (DAC) is one technology that can be used to do so [2]. However, there is great disparity between the scale of deployment required and the present position [3]. One of the critical factors that influences the performance of a DAC process are the CO₂ adsorption kinetics. The CO₂ adsorption kinetics, accounting for both the intraparticle CO₂ diffusion and CO₂ rate of adsorption/reaction, impact the productivity, energy consumption, and therefore capital and operating costs of a process [4, 5]. If the adsorption kinetics are not considered, the performance of a slow adsorbent could be greatly overestimated, and the costs underestimated. Rapid kinetics enable shorter cycle times, which in turn, results in higher productivity (tonnes of product per day, per tonne of adsorbent). Enhanced productivity means that a given amount of CO₂ can be captured with fewer contactor units, leading to reduced capital costs. Slow adsorption kinetics cause not only a decline in the aforementioned productivity, but may also hamper CO₂ recovery. For a given contactor size and feed gas velocity, slow kinetics result in a greater portion of that feed gas breaking through the bed, resulting in a loss of CO₂ back to the atmosphere. This can be compensated for by reducing the feed gas velocity, however, that further hampers the process productivity. With reduced CO₂ recovery, more feed gas needs to be processed to capture a given amount of CO₂, which results in greater energy consumption and operating costs. For these reasons, investigating and quantifying adsorption kinetics become critical to the deployment of adsorption-based DAC technologies.

The CO₂ adsorption kinetics can be experimentally measured at various scales; the crystal, the shaped adsorbent (e.g. pellet), or packed adsorption column, using a variety of techniques to extract diffusion coefficients (Figure 1) [6-8]. All experiments described here will also encompass any CO₂ reaction kinetics present in the adsorbent, though more comprehensive mathematical models and additional experiments may be needed to decouple the reaction kinetics from diffusion resistances. At the crystal scale, nuclear magnetic resonance (NMR) techniques such as pulsed field gradient (PFG) can track the diffusion of individual adsorbate molecules within the crystal, where attenuations in the NMR signal relate to molecular displacement [9]. Here, resistances due to micropore/surface diffusion (arising from

the transport of physically adsorbed molecules) are captured, and typically less than 10 mg of sample is needed. Shifts in the NMR peaks corresponding to the new reacted species and growth of the peaks over time can also allow for extraction of the reaction kinetics [10, 11]. At the pellet scale, techniques such as direct uptake/desorption rate measurements, zero length column measurements, and imaging utilise ~ 10 to 100 mg of sample and can account for both micropore and macropore resistances, where the latter comprises molecular diffusion, Knudsen diffusion, surface diffusion, and Poiseuille flow. Uptake/desorption rate measurements can often be done using commercial instruments either volumetrically, where the pressure change in the system is tracked over time, or gravimetrically, by measuring the mass change of the adsorbent over time after a stepwise introduction of the adsorbate [12]. The latter can be conducted using either constant pressure or constant volume experiments, though constant volume experiments require a correction to account for the changing driving force during the period of gas uptake. In the zero length column (ZLC) method, the desorption curve is tracked as a previously saturated adsorbent is exposed to a flow of inert gas. Here, the setup can be considered a perfectly mixed continuous flow cell and axial concentration gradients and heat transfer resistances are considered negligible [13]. It is also possible to directly track the diffusion of the adsorbate through the adsorbent pellet using imaging techniques such as interference microscopy (IFM), infra-red microscopy (IRM), and X-ray computed tomography (CT), which allow one to measure the internal transient concentration profile of the adsorbate in the adsorbent [14, 15]. Finally, one can also extract kinetic information from the breakthrough response of a column packed with an adsorbent (usually > 1 g) as the adsorbate is continuously flowed through the system [16]. At this scale, contributions from convection, axial dispersion, and external diffusion can be accounted for along with the aforementioned macropore and micropore diffusion resistances.

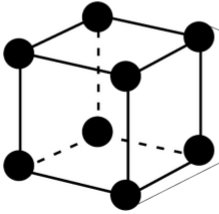
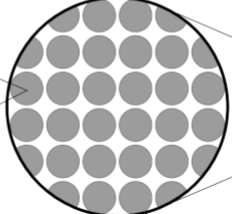
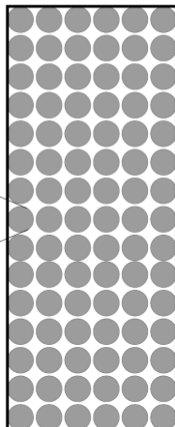
Adsorbent scale	Crystal (< 10 mg)	Pellet (10 - 100 mg)	Adsorption column (> 1 g)
			
Measurement technique	NMR	Direct uptake/desorption ZLC Imaging	Breakthrough
Reaction kinetics	✓	✓	✓
Mass transfer mechanisms	Micropore diffusion	Micropore diffusion Macropore diffusion	Micropore diffusion Macropore diffusion External diffusion Convection Axial dispersion

Figure 1. Schematic of the different adsorbent scales and their associated mass transfer mechanisms, measurement techniques, and sample masses.

In this study, we utilise a thermogravimetric analyser to conduct CO₂ uptake rate measurements at constant pressure for different adsorbents. This technique was chosen due to the ease of accessibility and the small sample mass required. To extract and quantify the adsorption kinetics for use in process modelling, the experimental data must be fitted to appropriate mathematical models. One of the simplest and most common ways to describe the CO₂ adsorption kinetics is with the linear driving force (LDF) model [17, 18]:

$$\frac{dq}{dt} = k_{LDF}(q_e - q) \quad (1)$$

where q is the amount of CO₂ adsorbed at time t , q_e is the CO₂ equilibrium adsorption capacity, and the linear driving force constant, k_{LDF} , is a lumped mass transfer coefficient accounting for both macropore and micropore diffusion resistances, as well as the rate of reaction in cases where chemisorption occurs. This model has been used in the literature to describe the adsorption kinetics of both chemisorbents (i.e.

amine-functionalised adsorbents) and physisorbents for DAC [19-23]. Other models used to describe the kinetics of DAC adsorbents include various rate order models (e.g. pseudo-first order (PFO), pseudo-second order (PSO), fractional order) [24-38], the Avrami model [27, 28, 30, 31, 33, 34, 36-39], combined PFO and Avrami [40], and reaction-mechanism based models [41, 42]. Modified forms of the shrinking core model have also been investigated, where the adsorbed phase is modelled as a product layer forming around a core of unreacted sorption sites, which shrinks as the reaction proceeds [43-45]. In contrast to the LDF model, one of the most rigorous methods to describe the kinetics within an adsorbent pellet is with the Fickian diffusion model [8, 18] given by equations (2) and (3):

$$J = -D \frac{\partial C}{\partial r} \quad (2)$$

$$D = B \left[\frac{d \ln P}{d \ln C} \right]_T \quad (3)$$

where J is the flux of the adsorbate, C is the adsorbate concentration, r is the radius of the adsorbent particle, P is the pressure, T is the temperature, D is the Fickian diffusivity, and B is the mobility of the adsorbate.

A separate term for the reaction kinetics would need to be included in the case of chemisorbents. It is mathematically/computationally intensive to incorporate this model into adsorption-based process simulations as the equations need to be repeatedly integrated at the pellet and column levels until cyclic steady state is achieved. Furthermore, since most processes will realistically operate under non-isothermal and non-isobaric conditions, these calculations would also have to be coupled with mass, heat, and energy balance equations across all scales. These factors aside, although equation (2) is a convenient mathematical representation, information as to how the diffusion coefficient is actually obtained is unclear or abstracted [46, 47]. For process modelling, simpler kinetic models such as the LDF model can be sufficient, as the information from a detailed kinetic model describing local rates of adsorption (i.e. spatial variation) within a pellet is often lost during the numerous integration/averaging steps [18]. There are some limitations to the LDF model when used for the modelling of rapid cycles [48-50], however, DAC cycles are not expected to operate in that way. For this work, we thus utilise the LDF model for quantification of our experimental adsorption kinetics.

Here, we analyse Lewatit VP OC 1065 (i.e. Lewatit), Purolite A110 (i.e. Purolite), and TIFSIX-3-Ni, as we previously highlighted these materials as promising adsorbents for DAC and reported many of their physicochemical and equilibrium sorption properties [51, 52]. In terms of their CO₂ adsorption kinetics, no data is currently available for Purolite and TIFSIX-3-Ni. For Lewatit, Young et al. fitted the LDF model to dynamic column breakthrough data, with experiments conducted at 25 °C, 50 °C, and 70 °C and 1%_{vol} CO₂ balanced with N₂, and reported a constant k_{LDF} of $3 \times 10^{-3} \text{ s}^{-1}$ within this temperature range [53]. Bos et al. measured the intrinsic adsorption kinetics of Lewatit in absence of transport limitations using a flat bed reactor at 5 °C to 40 °C and pure CO₂ pressures of 50, 100, and 200 mbar. They compared the use of the LDF model, quadratic driving force (QDF) model, and a Toth rate reaction model, and found that the Toth rate reaction model was best able to fit the CO₂ uptake data across the varying temperatures and pressures [54]. In that study, the reported k values for the LDF fitting of data measured at 50 mbar (i.e. 5%_{vol}) CO₂ ranged from $8 \times 10^{-2} \text{ s}^{-1}$ to $27.3 \times 10^{-2} \text{ s}^{-1}$ between 5 °C and 40 °C. Recently, Wu et al. measured the CO₂ uptake rate of Lewatit at 25 °C and 400 ppm (i.e. 0.04%_{vol}) CO₂ balanced with N₂ using a thermogravimetric analyser. The data was fitted to the Avrami model and a mass transfer coefficient (k_A) of $2.5 \times 10^{-4} \text{ s}^{-1}$ was reported [5]. The temperature dependence of the mass transfer coefficient remains unknown. For perspective, the k_{LDF} value for zeolite 13X beads of 1 mm in diameter at 10 °C at 1 mbar (i.e. 0.1%_{vol}) CO₂ is $1.6 \times 10^{-2} \text{ s}^{-1}$ [55]. Assuming the k_{LDF} value of $3 \times 10^{-3} \text{ s}^{-1}$ reported by Young et al. for Lewatit was also for bead sizes of 1 mm in diameter (Lewatit bead sizes range from 0.3 to 1.2 mm [56]), the adsorption kinetics of zeolite 13X is already a magnitude faster than that of Lewatit at 10 times lower CO₂ concentration and 15 °C lower temperature.

This study aims to fill the gaps in adsorption kinetics for Lewatit, Purolite and TIFSIX-3-Ni, and reports their temperature-dependent mass transfer coefficients at relevant DAC conditions. This work relies on using a thermogravimetric analyser to measure the mass of CO₂ adsorbed as a function of time at multiple temperatures for each adsorbent under a flow of 400 ppm CO₂, representative of dry ambient air. Following this approach, we then attempted to minimise any external mass transfer limitations as much as possible by modifying the thermogravimetric analyser sample holder. We then fitted the resulting experimental data simultaneously to a temperature-dependent LDF equation to obtain

temperature-dependent k_{LDF} constants, which can be used to describe the CO₂ adsorption kinetics of these materials in subsequent process models.

2. Experimental section

2.1 Adsorbent materials

Lewatit was purchased from Sigma-Aldrich, while Purolite was supplied by Purolite Ltd. UK. These resins are formed as spherical beads with particle sizes between 0.3 to 1.2 mm and containing up to 60 % water content [56, 57]. Further details of the material properties of these resins can be found in our previous work [51].

TIFSIX-3-Ni in powder and then pellet form was synthesised as described in our previous work [52]. For the experiments discussed here, ~ 400 mg of the powder sample referred to as “batch 5” in that work was used to form a 13 mm diameter pellet with ~ 5 mm thickness. To form these pellets, powdered TIFSIX-3-Ni was ground using a mortar and pestle and placed into a pellet die (13 mm evacuable stainless steel, Specac). This was positioned into a manual hydraulic press (Atlas™ Manual 15T, Specac) fitted with a low tonnage gauge conversion kit (0–1 t, Specac). A load of 0.5 t was applied and maintained for 45 s to form a pellet approximately 5 mm in height. The pellet was ejected with a small load applied to an extractor ring placed onto the base of the pellet die and cut into 9 pieces following a grid pattern. One of these pieces was then further cut into granules of ~ 1 to 2 mm in dimension to achieve similar particle sizes compared to the resin beads. Pellets were used in this study instead of powder as adsorbents in structured form would need to be used in an actual DAC process.

2.2 Kinetic sorption measurements

A NETZSCH TG 209 F1 Libra thermogravimetric analyser (TGA) was used to conduct all kinetic sorption measurements. A simplified schematic of the instrument is shown in Figure 2a. For each experiment, gas from a pure He cylinder (BOC, N5.0 grade) was used as the protective gas, which interacted with the balance system before entering the sample chamber. He gas was chosen instead of N₂ to minimise additional adsorption on the samples, especially for the physisorbent TIFSIX-3-Ni. Gas from a cylinder containing ~ 800 ppm CO₂ balanced with He (BOC, research grade) was used as the

sample gas, which entered above the balance and directly into the sample chamber. Here, the two gas streams mixed and interacted with the adsorbent sample in the crucible as they flowed up through the chamber and out of the top of the instrument. Three mixed gas cylinders were used to complete all measurements, whose CO₂ concentrations were 806 ppm, 832 ppm, and 834 ppm due to manufacturing variability. To create as close to a 400 ppm CO₂ in He environment within the sample chamber as possible to mimic dry ambient air, flow rate ratios between the mixed gas cylinder and pure He cylinder were varied between 0.9:1 to 1:1.

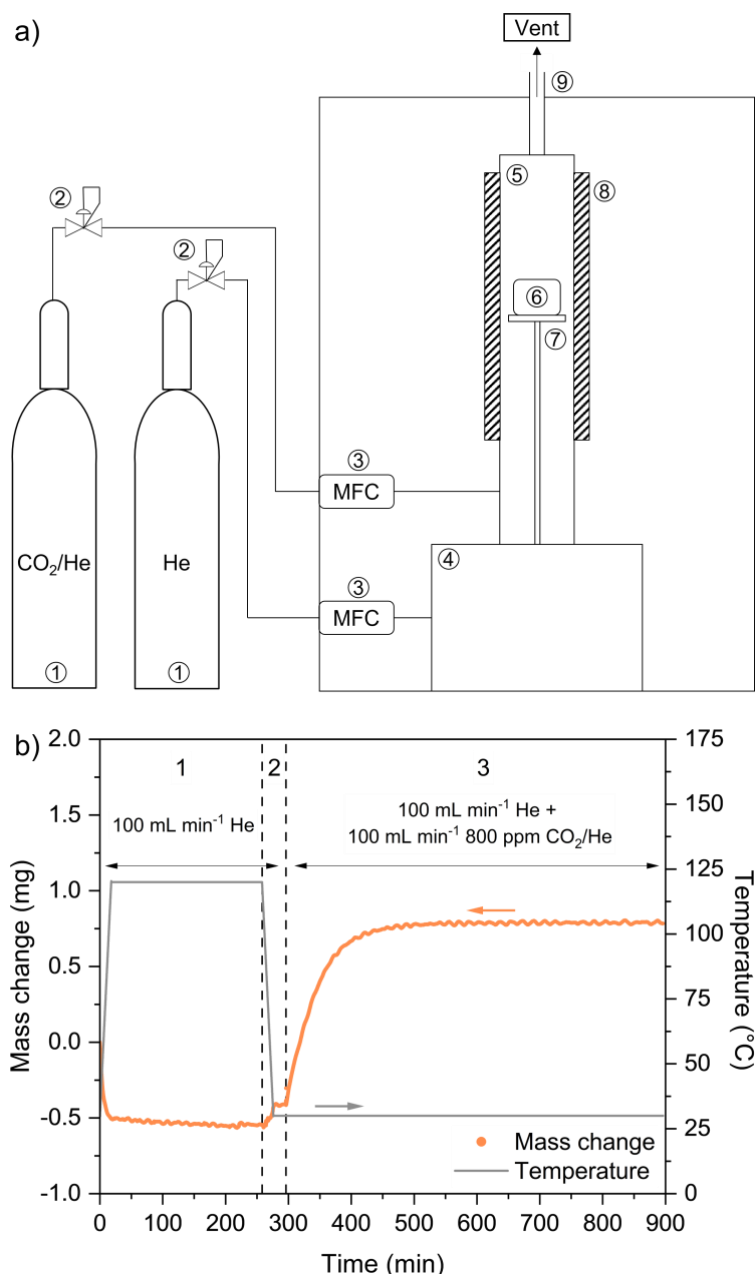


Figure 2. a) Simplified schematic of the set-up used for the kinetic sorption measurements, which includes (1) gas cylinders, (2) pressure reducing regulators, and a thermogravimetric analyser containing the following components: (3) mass flow controllers, (4) microbalance, (5) sample chamber, (6) crucible and (7) sample holder, (8) heating elements, and (9) gas outlet. b) Example of mass and temperature profiles over the course of a kinetic sorption measurement for a Purolite sample. Step 1: temperature increased from 30 to 120 °C and held for 4 h under a 100 mL min⁻¹ He flow. Step 2: temperature decreased back to 30 °C and held for 20 min under the same He flow. Step 3: a 100 mL min⁻¹ flow of the 800 ppm CO₂/He cylinder is then turned on for 10 h, at 30 °C.

A typical kinetic experiment consisted of three steps as shown in Figure 2b, during which the mass change of the sample was recorded as a function of time. First (step 1), sample was loaded into the TGA crucible and degassed under a flow of inert He gas until the mass remained stable. For experiments

using Lewatit and Purolite, ~ 25 to 30 mg of sample was heated from 30 °C to 120 °C at a rate of 5 °C min⁻¹ and held at this temperature for 4 h. For TIFSIX-3-Ni, ~ 15 mg to 20 mg of sample was heated from 30 °C to 160 °C at a rate of 5 °C min⁻¹ and held at this temperature for 2 h. 30 °C was chosen as the starting temperature for all experiments as it was difficult to consistently maintain a lower temperature. After this time, the temperature was decreased to the desired temperature for CO₂ adsorption and allowed to equilibrate for 20 min (step 2). In this work, experiments were conducted at adsorption temperatures of 30 °C, 45 °C, and 60 °C. Finally (step 3), the flow of CO₂ was turned on to achieve an overall gas stream of 400 ppm CO₂ balanced with He, and the mass change of the sample due to CO₂ adsorption was recorded as a function of time. A total flow rate of 200 mL min⁻¹ was used for the measurements. For Lewatit and Purolite, samples were exposed to 400 ppm CO₂ flow for 10 h, 6 h, and 4 h at 30 °C, 45 °C, and 60 °C, respectively, and a fresh sample was used for each measurement. For TIFSIX-3-Ni, the same sample was exposed to 400 ppm CO₂ flow for 3 h, 2.5 h, and 2 h at 30 °C, 45 °C, and 60 °C, respectively. These times were chosen to ensure that saturation of the sample would be achieved within this period, i.e. when the mass reaches a plateau. Three experiments were repeated at each temperature.

Prior to the measurements, samples were degassed ex-situ overnight using a Micromeritics VacPrepTM 061 at 0.02 mbar and either 120 °C (Lewatit and Purolite) or 160 °C (TIFSIX-3-Ni), with the temperature increased from room temperature at a rate of 10 °C min⁻¹ for the latter. A correction run with an empty crucible and identical analysis conditions was also performed before each measurement to account for buoyancy effects. We note that oscillations in the TGA mass signal, as can be seen in Figure 2b, sometimes occurred during experiments for both correction and sample measurements for indeterminate reasons (see Figures S1 to S3), but this did not significantly impact subsequent fitting and analysis procedures.

2.3 Data analysis

To calculate the k_{LDF} constant for each experiment, the data collected in step 3 of the procedure discussed above was first adjusted to the mass of CO₂ adsorbed as a function of time, with both mass and time starting at 0. This was then converted to a fractional uptake using equation (4):

$$f(t) = \frac{m(t) - m_{initial}}{m_{final} - m_{initial}} \quad (4)$$

where $f(t)$ is the fractional mass uptake between 0 and 1 as a function of time t , $m(t)$ is the mass of CO₂ adsorbed at a given t , $m_{initial}$ is the mass of CO₂ adsorbed at $t = 0$, i.e. $m_{initial} = 0$, and m_{final} is the average mass of CO₂ adsorbed in the last 30 min of the experiment.

This data was then fitted to an exponential form of the LDF model (equation 5) [18] using the non-linear curve fit function in OriginPro with the orthogonal distance regression iteration algorithm to give the k_{LDF} constant:

$$f(t) = 1 - e^{-k_{LDF}t} \quad (5)$$

To compare the effect of different temperatures, a temperature dependence of the k_{LDF} constant was described using the Arrhenius equation shown in equation (6):

$$k_{LDF}(T) = k_0 \exp\left(\frac{-E_a}{RT}\right) \quad (6)$$

where k_0 is the pre-exponential factor (or k_{LDF} at infinite temperature), E_a is the commonly called activation energy for mass transfer (though we note that not all mechanisms are necessarily activated), R is the universal gas constant, and T is the temperature.

To determine this temperature dependence for each adsorbent, fractional uptake curves repeated at each temperature were averaged at each time data point, and the resulting mean $f(t)$ data set at each temperature were fitted simultaneously to equation (5) and an alternative form of the Arrhenius equation shown as equation (7):

$$k_{LDF}(T) = \exp\left[\ln(k_0) - \frac{E_a}{RT}\right] \quad (7)$$

with the standard deviation at each time point used to weight the fitting. $\ln(k_0)$ and E_a were obtained as fitted parameters with associated uncertainty bounds for a 95% confidence interval which could then be used to calculate $k_{LDF}(T)$. The fitting procedure was again done using the non-linear curve fit function in OriginPro with the orthogonal distance regression iteration algorithm.

3. Results and discussion

3.1 Optimisation of experimental factors for kinetic sorption measurements

As mentioned previously, the k_{LDF} constant is an overall mass transfer coefficient describing the CO₂ adsorption kinetics, which accounts for both the CO₂ intraparticle diffusion and CO₂ rate of adsorption/reaction. In other words, any differences in the k_{LDF} constants should only be due to the adsorbent itself and not affected by external mass transfer limitations. For our experimental set-up, we assumed that the sample masses used (~ 15 to 30 mg) were sufficiently low to avoid any bed or heat transfer effects. Calculations were also subsequently conducted to confirm our operation in near isothermal conditions (see SI for details). In addition, the constant pressure approach used in this work requires the bulk gas phase composition to remain constant, therefore, one must ensure that gas around the sample is adequately refreshed and not depleted of CO₂. This can be affected by the gas flow path in the instrument (not within user control), the dimensions of the crucible containing the sample, and the gas flow rate.

The standard alumina crucibles are only open to fluid flow at the top and therefore not ideal for the envisioned measurements. As explained in Section 2.2, gas flows from the bottom and up through this TGA's sample chamber, which prevents a good mixing with the sample when using a standard crucible. In this scenario, the gas only flows around the crucible and directly interacts with the top layer of sample particles, before diffusing through the crucible to reach the particles below. As a result, the calculated k_{LDF} would be an underestimation.

To optimise the gas flow through the sample, we employed an aluminium crucible modified by drilling 0.2 mm holes at the base with a 0.5 mm square pitch. This was meant to allow gas flow through the sample, rather than around the crucible. A significant proportion of these drilled holes on the base however would have been blocked by the TGA sample holder platform. Hence, to further optimise the

set-up, a makeshift basket made of perforated stainless steel was formed in which the aluminium crucible could be placed. The rim of the crucible rests on the edge of the basket and elevates the base of the crucible from the sample holder platform. Photographs of all three crucible iterations are shown below in Figure 3a.

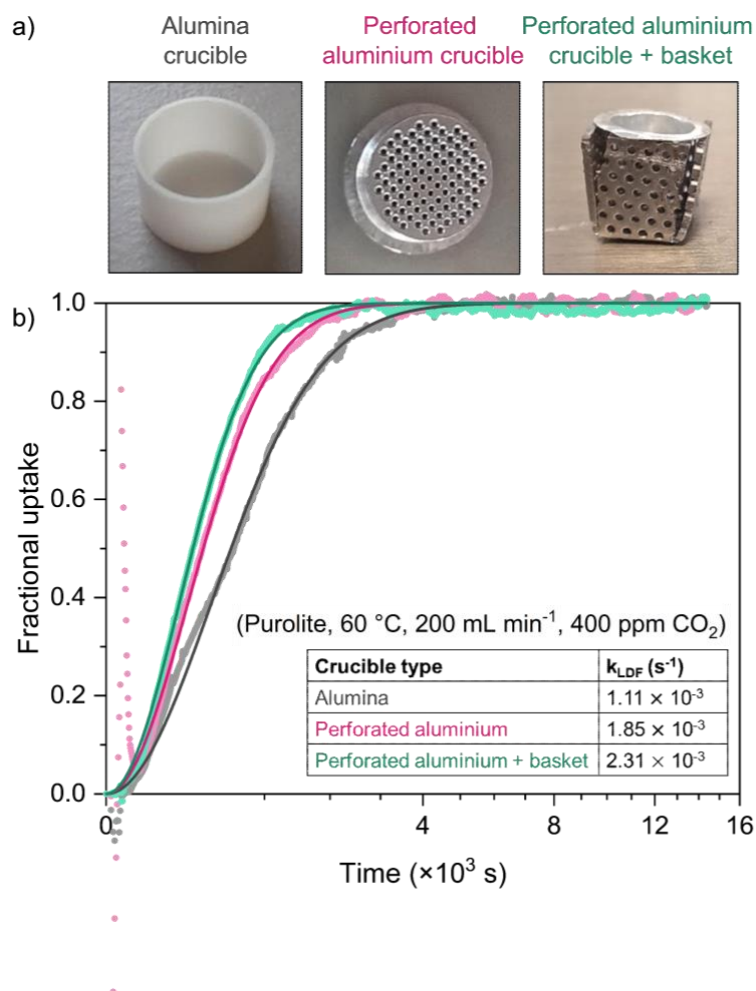


Figure 3. a) Photographs of the standard alumina crucible, perforated aluminium crucible, and perforated aluminium crucible in the makeshift basket. b) Comparison of the experimental (filled circles) and fitted (solid lines) fractional uptakes and corresponding k_{LDF} constants of Purolite samples measured using the standard alumina crucible, perforated aluminium crucible, and perforated aluminium crucible in the makeshift basket. Time is plotted on a square root scale for clarity.

To test each set-up (i.e. standard alumina crucible, perforated aluminium crucible, and perforated aluminium crucible with a makeshift basket), we conducted TGA measurements on samples of Purolite at 60 °C under a total flow rate of 200 mL min⁻¹ of 400 ppm CO₂ balanced with He (Figure 3b). We chose to use 60 °C since the adsorption kinetics would be fastest at this temperature amongst our selected range, thus any impacts of external mass transfer resistance would be amplified. As seen from

Figure 3b, using the perforated aluminium crucible with the makeshift basket allowed for the fastest CO₂ adsorption kinetics. This set-up was therefore used for all further experiments. We note some sharp spikes/dips in the experimental fractional uptake, particularly for the perforated aluminium crucible during the first few seconds of step 3. This is likely an artefact of the sudden introduction of CO₂, and was also sometimes observed in subsequent experiments (Figures S1 to S3). However, these experimental discrepancies did not significantly affect the fitting of the k_{LDF} constant. Overall, these modifications improved the mixing of gas with the sample and reduced any mass transfer limitations due to the crucible as much as possible.

3.2 Temperature-dependent kinetic sorption measurements

For process modelling, a temperature-dependent k_{LDF} constant should be determined for adsorbents of interest, as it allows accurate modelling of the kinetics throughout the entire cycle (i.e. adsorption, desorption, and transition steps). Similarly, the dependence of the k_{LDF} values on the CO₂ concentration should also be investigated since the CO₂ concentration may vary along the length of the column as gas is adsorbed. However, in this work we focused our experiments on the initial feed gas concentration in a DAC process of 400 ppm CO₂. To obtain a temperature-dependent k_{LDF} for Lewatit, Purolite, and TIFSIX-3-Ni, we carried out experiments as described in Section 2.2 for each adsorbent at 30 °C, 45 °C, and 60 °C, with a total flow rate of 200 mL min⁻¹ of 400 ppm CO₂ balanced with He using the perforated aluminium crucible with a stainless-steel basket. For each adsorbent, three experiments were repeated at each of the three temperatures, and subsequent data analysis was conducted following the procedure outlined in Section 2.3. The experimental and fitted $f(t)$ data for these measurements are shown in Figures S1 to S3. The fitted parameter values for $\ln(k_0)$ and E_a are shown below in Table 1, along with associated uncertainty bounds for a 95% confidence interval. These parameters are then used to calculate k_{LDF} as a function of temperature, and their uncertainty bounds can be propagated to determine uncertainty bounds on $k_{LDF}(T)$ (see SI for details). These fitted results are shown in Figure 4, with an extrapolation of 10 °C above and below the measured temperature range.

Table 1. Fitting parameters for equation (5) with uncertainty bounds for a 95% confidence interval for Lewatit, Purolite, and TIFSIX-3-Ni. k_0 is the pre-exponential factor (or k_{LDF} at infinite temperature) of the Arrhenius equation and E_a is the activation energy for mass transfer.

	$\ln(k_0)$ (s^{-1})	E_a ($kJ\ mol^{-1}$)
Lewatit	4.987 ± 0.055	32.90 ± 0.14
Purolite	11.00 ± 0.09	47.89 ± 0.25
TIFSIX-3-Ni	6.778 ± 0.174	33.79 ± 0.44

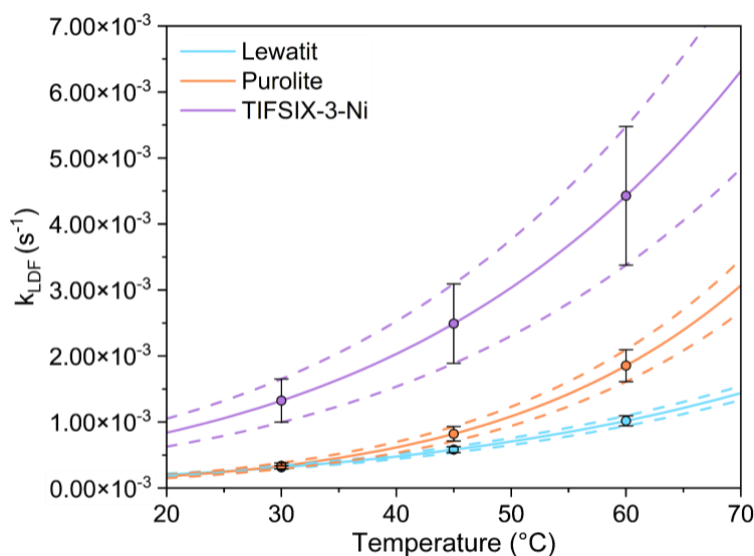


Figure 4. Comparison of temperature-dependent k_{LDF} constants with uncertainty bounds (dashed lines) for a 95% confidence interval between 20 and 70 °C for Lewatit, Purolite, and TIFSIX-3-Ni. Individual data points indicate the temperatures at which k_{LDF} constants were experimentally measured.

The two resins, Lewatit and Purolite, exhibit similar k_{LDF} constants up to 40 °C, with values of $4.76 \times 10^{-4} s^{-1}$ and $6.14 \times 10^{-4} s^{-1}$, respectively at this temperature. As the temperature increases beyond 40 °C, Purolite begins to have significantly faster adsorption kinetics compared to Lewatit. The kinetic resistances dependent on temperature are molecular diffusion ($T^{1.7}$ dependence), Knudsen diffusion ($T^{1/2}$ dependence), surface diffusion, and the rate of chemical reaction (both $e^{-E_a/RT}$ dependence) [8]. Therefore, one or more of these resistances may be more dominant in Purolite compared to Lewatit, though the dominant resistance may change throughout our measured temperature range. Since the k_{LDF} of Purolite increases faster with temperature than Lewatit, this may suggest a lower activation energy for surface diffusion and/or reaction in Purolite.

At 25 °C, we calculated the k_{LDF} for Lewatit to be $2.52 \times 10^{-4} \text{ s}^{-1}$. This agrees well with the k_A value of $2.5 \times 10^{-4} \text{ s}^{-1}$ reported by Wu et al. [cite] for Lewatit, who fitted their TGA uptake data measured at 25 °C and 400 ppm CO₂ to the Avrami model given by equation (8):

$$q = q_e(1 - e^{-(k_A t)^n}) \quad (8)$$

where q is the amount of CO₂ adsorbed at time t , q_e is the CO₂ equilibrium adsorption capacity, k_A is the Avrami mass transfer coefficient, and n is the Avrami constant.

Since the authors reported an n value of 0.9710 (i.e. close to 1), k_A can be roughly compared to k_{LDF} .

In another comparison, Young et al. reported a constant k_{LDF} of 0.003 s^{-1} for Lewatit at 1%_{vol} (or 10,000 ppm) CO₂ concentration between 25 and 70 °C [53], which represents an order of magnitude difference between our results at 25 °C. This discrepancy is likely due to the difference in CO₂ concentration, as Lewatit is a macroporous resin and thus it is likely there is a mass transfer resistance arising from macropore diffusion, which is impacted by the gas phase concentration. Indeed, Bos et al. previously reported a concentration dependence of the CO₂ adsorption kinetics for Lewatit, where the CO₂ uptake of Lewatit was faster with pure CO₂ compared to 50% and 25% CO₂ diluted with N₂ [54]. Therefore, it is important for future studies to conduct their kinetic sorption experiments at the relevant CO₂ concentrations for DAC to achieve accurate kinetic estimations. We also note that Young et al. performed dynamic column breakthrough experiments with ~ 200 mg of sample and assumed isothermal operation of their column [53], where any changes in the temperature of the adsorbent would not be accounted for and could result in an inflated k_{LDF} .

TIFSIX-3-Ni displays significantly faster adsorption kinetics compared to Lewatit and Purolite over the 20 °C to 70 °C temperature range, ranging from 8.38×10^{-4} to $6.32 \times 10^{-3} \text{ s}^{-1}$. We hypothesise that this is due to the absence of reaction kinetics in TIFSIX-3-Ni as it is a physisorbent, resulting in an overall faster CO₂ adsorption rate. In terms of the intraparticle diffusion, there is likely a contribution of both micropore and macropore diffusion due to the intrinsic ultramicropores in TIFSIX-3-Ni and pelletisation of the sample, respectively, though our experiments do not allow us to quantify the contribution of each resistance. As a result, we cannot directly compare the impact of intraparticle diffusion between TIFSIX-3-Ni and the macroporous resins.

We also calculated the average equilibrium CO₂ loading for the TGA experiments conducted at each temperature (see SI for details). We compared these to the CO₂ loadings calculated from the CO₂ isotherm fitting model parameters determined from volumetric sorption experiments using a Micromeritics 3Flex porosity analyser discussed in our previous works [51, 52]. This analysis helps to verify that the equilibrium results from the TGA are indeed reasonable, and that subsequently the kinetic results which rely on the final equilibrium loading should be reliable as well. The CO₂ isotherm models and their fitted parameters are provided in the SI. As seen from Figure 5, the average loadings determined from the two methods are in relatively good agreement at 45 °C and 60 °C (~ 5% to 20% difference, except for ~ 30% difference for TIFSIX-3-Ni at 60 °C), while there is a larger discrepancy between the averaged results at 30 °C (~ 20% to 35% difference). The temperature calibration for the TGA used in this study was performed using elements with relatively high melting points (~ 150 °C to 1110 °C), and so the temperature control may not be as accurate at 30 °C compared to higher temperatures. Fluctuations in the TGA balance reading as observed in Figures S1 to S3 were likely another source of error. In comparison, the porosity analyser used for the volumetric sorption experiments could achieve better resolution, better sample activation (degassed in-situ at 120 °C and 0.00002 mbar for 24 h), and experimental checks were done in our previous work to ensure that equilibrium was indeed reached during measurements. Overall however, the results from the two methods are relatively comparable with almost all error bars overlapping, and are in better agreement with increasing temperature.

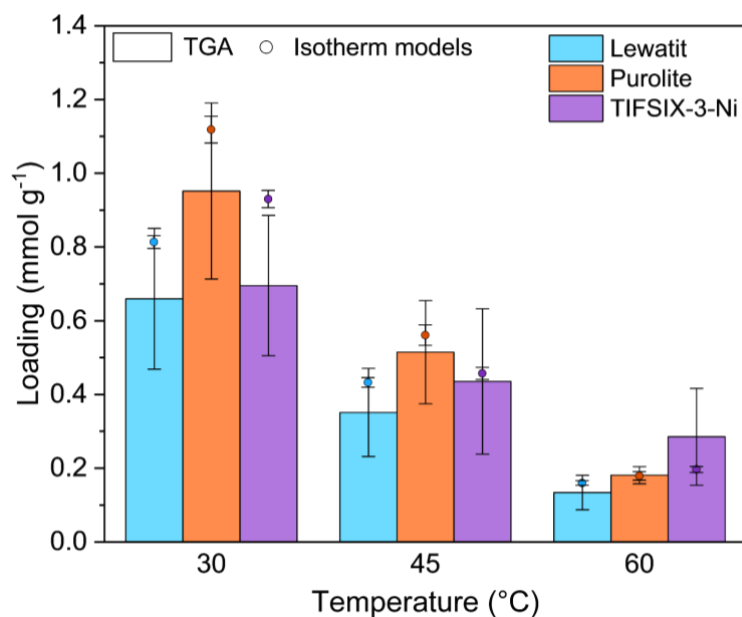


Figure 5. Comparison of the averaged equilibrium CO₂ loadings for Lewatit, Purolite, and TIFSIX-3-Ni at 30 °C, 45 °C, and 60 °C and 400 ppm CO₂ concentration determined from TGA experiments and CO₂ sorption isotherm models with error bars for a 95% confidence interval.

4. Conclusions and future work

This work provides a quantitative evaluation, under DAC conditions (i.e. 400 ppm CO₂), of the temperature-dependent linear driving force constants, $k_{LDF}(T)$, for three promising DAC adsorbents, Lewatit VP OC 1065, Purolite A110, and TIFSIX-3-Ni. We measured the mass of CO₂ adsorbed over time using a thermogravimetric analyser from a flow of 400 ppm CO₂ balanced with He at 30 °C, 45 °C, and 60 °C, and fitted the experimental data using the linear driving force model. To ensure the accuracy of the method, we minimised external mass transfer limitations by adapting the experimental set-up, i.e. sample holder.

The results show that TIFSIX-3-Ni displays faster adsorption kinetics than the resins between 20 °C to 70 °C. At 25 °C, the k_{LDF} constant for TIFSIX-3-Ni is $1.13 \times 10^{-3} \text{ s}^{-1}$, compared to $2.36 \times 10^{-4} \text{ s}^{-1}$ and $2.77 \times 10^{-4} \text{ s}^{-1}$ for Lewatit and Purolite, respectively. We attribute this to the lack of chemical reaction with CO₂ as TIFSIX-3-Ni is a physisorbent, resulting in a faster CO₂ rate of adsorption compared to the resins which have additional resistance from their reaction kinetics. Purolite and Lewatit have comparable kinetics up to 40 °C, after which Purolite exhibits faster kinetics than Lewatit, potentially due to a smaller activation energy for surface diffusion and/or reaction rate.

In terms of future work, additional experiments should be done if k_{LDF} constants at temperatures below 20 °C or above 70 °C are desired, rather than relying on further extrapolation. Our k_{LDF} values are also only valid at a CO₂ concentration of 400 ppm, however the CO₂ concentration may vary along the length of the column as gas is adsorbed. Therefore, additional kinetic measurements should be conducted which account for variations in concentration, either by repeating the procedure used in this work at multiple CO₂ concentrations, or using a different experimental methodology from which the micropore and macropore resistances can be extracted, such as the zero length column method [13, 58]. Overall, the $k_{LDF}(T)$ values determined in this work can now be used for initial process scale modelling to assess the process performance of Lewatit, Purolite, and TIFSIX-3-Ni for DAC.

Supporting Information

The Supporting Information includes: experimental fractional uptake curves and corresponding fitting results; procedures for error propagation; procedures for equilibrium loading calculations from TGA experiments; CO₂ isotherm models and corresponding fitted parameters used to calculate equilibrium loadings from previous volumetric experiments.

Acknowledgements

The authors would like to acknowledge Imperial College London for the President's PhD Scholarship (MYL, CP), funding provided by UK Research and Innovation (UKRI) under grants EP/P026214/1 (DD, CP) and EP/T033940/1 (DD), and the support via the Eric and Wendy Schmidt AI in Science Postdoctoral Fellowship, a Schmidt Futures program (DD).

Conflict of Interest

The authors declare no competing financial interest.

References

- [1] P. A. Arias *et al.*, "Climate Change 2021: The Physical Science Basis. Contribution of Working Group I to the Sixth Assessment Report of the Intergovernmental Panel on Climate Change," IPCC, 2021.
- [2] "Direct Air Capture." International Energy Agency. <https://www.iea.org/energy-system/carbon-capture-utilisation-and-storage/direct-air-capture> (accessed 2024).
- [3] S. M. Smith *et al.*, "The State of Carbon Dioxide Removal - 1st Edition," The State of Carbon Dioxide Removal, 2023. [Online]. Available: <http://dx.doi.org/10.17605/OSF.IO/W3B4Z>
- [4] J. Young, F. McIlwaine, B. Smit, S. Garcia, and M. van der Spek, "Process-informed adsorbent design guidelines for direct air capture," *Chemical Engineering Journal*, vol. 456, 2023, doi: 10.1016/j.cej.2022.141035.
- [5] J. Wu, X. Zhu, Y. Chen, R. Wang, and T. Ge, "The analysis and evaluation of direct air capture adsorbents on the material characterization level," *Chemical Engineering Journal*, vol. 450, 2022, doi: 10.1016/j.cej.2022.137958.
- [6] D. M. Ruthven, J. Kärger, S. Brandani, and E. Mangano, "Sorption kinetics: measurement of surface resistance," *Adsorption*, vol. 27, no. 5, pp. 787-799, 2020, doi: 10.1007/s10450-020-00257-w.
- [7] D. M. Ruthven and M. F. M. Post, "Chapter 12 Diffusion in zeolite molecular sieves," in *Introduction to Zeolite Science and Practice*, (Studies in Surface Science and Catalysis, 2001, pp. 525-577.
- [8] D. M. Ruthven, *Principles of Adsorption and Adsorption Processes*. John Wiley & Sons, 1984.
- [9] J. Kärger, M. Avramovska, D. Freude, J. Haase, S. Hwang, and R. Valiullin, "Pulsed field gradient NMR diffusion measurement in nanoporous materials," *Adsorption*, vol. 27, no. 3, pp. 453-484, 2021, doi: 10.1007/s10450-020-00290-9.
- [10] Y. Wu, C. D'Agostino, D. J. Holland, and L. F. Gladden, "In situ study of reaction kinetics using compressed sensing NMR," *Chem Commun (Camb)*, vol. 50, no. 91, pp. 14137-40, Nov 25 2014, doi: 10.1039/c4cc06051b.
- [11] A. H. Berge *et al.*, "Revealing carbon capture chemistry with 17-oxygen NMR spectroscopy," *Nat Commun*, vol. 13, no. 1, p. 7763, Dec 15 2022, doi: 10.1038/s41467-022-35254-w.
- [12] J.-Y. Wang, E. Mangano, S. Brandani, and D. M. Ruthven, "A review of common practices in gravimetric and volumetric adsorption kinetic experiments," *Adsorption*, vol. 27, no. 3, pp. 295-318, 2020, doi: 10.1007/s10450-020-00276-7.
- [13] S. Brandani and E. Mangano, "The zero length column technique to measure adsorption equilibrium and kinetics: lessons learnt from 30 years of experience," *Adsorption*, vol. 27, no. 3, pp. 319-351, 2020, doi: 10.1007/s10450-020-00273-w.
- [14] J. Karger *et al.*, "Microimaging of transient guest profiles to monitor mass transfer in nanoporous materials," *Nat Mater*, vol. 13, no. 4, pp. 333-43, Apr 2014, doi: 10.1038/nmat3917.
- [15] R. Pini, L. Joss, and S. A. Hosseinzadeh Hejazi, "Quantitative imaging of gas adsorption equilibrium and dynamics by X-ray computed tomography," *Adsorption*, vol. 27, no. 5, pp. 801-818, 2020, doi: 10.1007/s10450-020-00268-7.
- [16] N. S. Wilkins, A. Rajendran, and S. Farooq, "Dynamic column breakthrough experiments for measurement of adsorption equilibrium and kinetics," *Adsorption*, vol. 27, no. 3, pp. 397-422, 2020, doi: 10.1007/s10450-020-00269-6.
- [17] E. Glueckauf, "Theory of chromatography. Part 10.—Formulæ for diffusion into spheres and their application to chromatography," *Trans. Faraday Soc.*, vol. 51, no. 0, pp. 1540-1551, 1955, doi: 10.1039/tf9555101540.
- [18] S. Sircar and J. R. Hufton, "Why Does the Linear Driving Force Model for Adsorption Kinetics Work?," *Adsorption*, vol. 6, no. 2, pp. 137-147, 2000, doi: 10.1023/a:1008965317983.
- [19] S. M. W. Wilson and F. H. Tezel, "Direct Dry Air Capture of CO₂ Using VTSA with Faujasite Zeolites," *Industrial & Engineering Chemistry Research*, vol. 59, no. 18, pp. 8783-8794, 2020, doi: 10.1021/acs.iecr.9b04803.

- [20] B. M. Balasubramaniam, P.-T. Thierry, S. Lethier, V. Pugnet, P. Llewellyn, and A. Rajendran, "Process-performance of solid sorbents for Direct Air Capture (DAC) of CO₂ in optimized temperature-vacuum swing adsorption (TVSA) cycles," *Chemical Engineering Journal*, vol. 485, 2024, doi: 10.1016/j.cej.2024.149568.
- [21] Q. Grossmann, V. Stampi-Bombelli, A. Yakimov, S. Docherty, C. Coperet, and M. Mazzotti, "Developing Versatile Contactors for Direct Air Capture of CO₂ through Amine Grafting onto Alumina Pellets and Alumina Wash-Coated Monoliths," *Ind Eng Chem Res*, vol. 62, no. 34, pp. 13594-13611, Aug 30 2023, doi: 10.1021/acs.iecr.3c01265.
- [22] V. Stampi-Bombelli, M. van der Spek, and M. Mazzotti, "Analysis of direct capture of CO₂ from ambient air via steam-assisted temperature–vacuum swing adsorption," *Adsorption*, vol. 26, no. 7, pp. 1183-1197, 2020, doi: 10.1007/s10450-020-00249-w.
- [23] H. Liu, H. Lin, S. Dai, and D.-e. Jiang, "Minimal Kinetic Model of Direct Air Capture of CO₂ by Supported Amine Sorbents in Dry and Humid Conditions," *Industrial & Engineering Chemistry Research*, 2024, doi: 10.1021/acs.iecr.3c04535.
- [24] C. Hou, Y. Wu, T. Wang, X. Wang, and X. Gao, "Preparation of Quaternized Bamboo Cellulose and Its Implication in Direct Air Capture of CO₂," *Energy & Fuels*, vol. 33, no. 3, pp. 1745-1752, 2018, doi: 10.1021/acs.energyfuels.8b02821.
- [25] W. Si *et al.*, "Kinetics and mechanism of low-concentration CO₂ adsorption on solid amine in a humid confined space," *The Canadian Journal of Chemical Engineering*, vol. 97, no. 3, pp. 697-701, 2018, doi: 10.1002/cjce.23257.
- [26] T. Wang, X. Wang, C. Hou, and J. Liu, "Quaternary functionalized mesoporous adsorbents for ultra-high kinetics of CO₂ capture from air," *Sci Rep*, vol. 10, no. 1, p. 21429, Dec 8 2020, doi: 10.1038/s41598-020-77477-1.
- [27] W. Wang, F. Liu, Q. zhang, G. Yu, and S. Deng, "Efficient removal of CO₂ from indoor air using a polyethyleneimine-impregnated resin and its low-temperature regeneration," *Chemical Engineering Journal*, vol. 399, 2020, doi: 10.1016/j.cej.2020.125734.
- [28] Y. Miao, Z. He, X. Zhu, D. Izikowitz, and J. Li, "Operating temperatures affect direct air capture of CO₂ in polyamine-loaded mesoporous silica," *Chemical Engineering Journal*, vol. 426, 2021, doi: 10.1016/j.cej.2021.131875.
- [29] L. Qi *et al.*, "Role of brush-like additives in CO₂ adsorbents for the enhancement of amine efficiency," *Journal of Environmental Chemical Engineering*, vol. 9, no. 6, 2021, doi: 10.1016/j.jece.2021.106709.
- [30] M. Modayil Korah *et al.*, "Electrospun Poly(vinyl alcohol)–l-Arginine Nanofiber Composites for Direct Air Capture of CO₂," *ACS ES&T Engineering*, vol. 3, no. 3, pp. 373-386, 2022, doi: 10.1021/acsestengg.2c00307.
- [31] A. A. Al-Absi, M. Mohamedali, A. Domin, A. M. Benneker, and N. Mahinpey, "Development of in situ polymerized amines into mesoporous silica for direct air CO₂ capture," *Chemical Engineering Journal*, vol. 447, 2022, doi: 10.1016/j.cej.2022.137465.
- [32] C. Zhang, S. Sun, S. He, and C. Wu, "Direct air capture of CO₂ by KOH-activated bamboo biochar," *Journal of the Energy Institute*, vol. 105, pp. 399-405, 2022, doi: 10.1016/j.joei.2022.10.017.
- [33] S. Wang, Y. Liu, C. Zhang, S. Guo, and Y. Li, "High Gravity-Enhanced Direct Air Capture: A Leap Forward in CO₂ Adsorption Technology," *Atmosphere*, vol. 15, no. 2, 2024, doi: 10.3390/atmos15020238.
- [34] S. Wang, Y. Liu, C. Zhang, S. Guo, Y. Li, and S. Cheng, "The amine-functionalized alumina captures CO₂ directly from the ambient air in the rotating adsorption bed," *Chemical Engineering and Processing - Process Intensification*, vol. 199, 2024, doi: 10.1016/j.cep.2024.109735.
- [35] F. Liu, T. Wang, H. Dong, and W. Liu, "Modified metal–organic framework by a novel coordinatively unsaturated amine grafting mechanism for direct air capture of CO₂," *Chemical Engineering Journal*, vol. 454, 2023, doi: 10.1016/j.cej.2022.140431.
- [36] L. Samaddoost, M. Soltani, E. Fatehifar, and E. Abbasi Asl, "Design of amine-functionalized resin via a facial method with efficient CO₂ capture from air," *Process Safety and Environmental Protection*, vol. 171, pp. 18-27, 2023, doi: 10.1016/j.psep.2023.01.008.

- [37] N. T. D. Hanh *et al.*, "Dynamic kinetic studies of CO₂ capture using polyethyleneimine-modified cylindrical NaY zeolite in packed beds under ambient conditions," *Journal of the Taiwan Institute of Chemical Engineers*, vol. 156, 2024, doi: 10.1016/j.jtice.2024.105366.
- [38] J. R. Hoffman, A. E. Baumann, and C. M. Stafford, "Thickness Dependent CO₂ Adsorption of Poly(ethyleneimine) Thin Films for Direct Air Capture," *Chem Eng J*, vol. 481, Feb 2024, doi: 10.1016/j.cej.2023.148381.
- [39] Y. Wang *et al.*, "Additives enhancing supported amines performance in CO₂ capture from air," *SusMat*, vol. 3, no. 3, pp. 416-430, 2023, doi: 10.1002/sus2.141.
- [40] L. A. Darunte *et al.*, "Moving Beyond Adsorption Capacity in Design of Adsorbents for CO₂ Capture from Ultradilute Feeds: Kinetics of CO₂ Adsorption in Materials with Stepped Isotherms," *Industrial & Engineering Chemistry Research*, vol. 58, no. 1, pp. 366-377, 2018, doi: 10.1021/acs.iecr.8b05042.
- [41] J. Elfving and T. Sainio, "Kinetic approach to modelling CO₂ adsorption from humid air using amine-functionalized resin: Equilibrium isotherms and column dynamics," (in English), *Chemical Engineering Science*, vol. 246, Dec 31 2021, doi: 10.1016/j.ces.2021.116885.
- [42] W. Jung, J. Park, and K. S. Lee, "Kinetic modeling of CO₂ adsorption on an amine-functionalized solid sorbent," (in English), *Chemical Engineering Science*, vol. 177, pp. 122-131, Feb 23 2018, doi: 10.1016/j.ces.2017.11.003.
- [43] C. Hou *et al.*, "Porosity and hydrophilicity modulated quaternary ammonium-based sorbents for CO₂ capture," *Chemical Engineering Journal*, vol. 413, 2021, doi: 10.1016/j.cej.2020.127532.
- [44] T. Wang, J. Liu, H. Huang, M. Fang, and Z. Luo, "Preparation and kinetics of a heterogeneous sorbent for CO₂ capture from the atmosphere," *Chemical Engineering Journal*, vol. 284, pp. 679-686, 2016, doi: 10.1016/j.cej.2015.09.009.
- [45] A. Wallace, Y. Ren, C. W. Jones, and R. P. Lively, "Kinetic model describing self-limiting CO₂ diffusion in supported amine adsorbents," *Chemical Engineering Journal*, vol. 472, 2023, doi: 10.1016/j.cej.2023.144838.
- [46] J. Kärger and D. M. Ruthven, "Diffusion in nanoporous materials: fundamental principles, insights and challenges," *New Journal of Chemistry*, vol. 40, no. 5, pp. 4027-4048, 2016, doi: 10.1039/c5nj02836a.
- [47] S. Sircar, "Adsorbate mass transfer into porous adsorbents – A practical viewpoint," *Separation and Purification Technology*, vol. 192, pp. 383-400, 2018, doi: 10.1016/j.seppur.2017.10.014.
- [48] E. Alpay and D. M. Scott, "The linear driving force model for fast-cycle adsorption and desorption in a spherical particle," *Chemical Engineering Science*, vol. 47, no. 2, pp. 499-502, 1992, doi: 10.1016/0009-2509(92)80041-a.
- [49] D. M. Scott, "The linear driving force model for cyclic adsorption and desorption: the effect of shape," *Chemical Engineering Science*, vol. 49, no. 6, pp. 914-916, 1994, doi: 10.1016/0009-2509(94)80028-6.
- [50] M. I. Hossain, A. D. Ebner, and J. A. Ritter, "New linear driving force correlation spanning long and short cycle time pressure swing adsorption processes," *Adsorption*, vol. 22, no. 7, pp. 939-950, 2016, doi: 10.1007/s10450-016-9801-1.
- [51] M. A. Low, D. Danaci, H. Azzan, R. T. Woodward, and C. Petit, "Measurement of Physicochemical Properties and CO₂, N₂, Ar, O₂, and H₂O Unary Adsorption Isotherms of Purolite A110 and Lewatit VP OC 1065 for Application in Direct Air Capture," *J Chem Eng Data*, vol. 68, no. 12, pp. 3499-3511, Dec 14 2023, doi: 10.1021/acs.jced.3c00401.
- [52] M.-Y. Low *et al.*, "Physicochemical properties, equilibrium adsorption performance, manufacturability, and stability of TIFSIX-3-Ni for direct air capture," *ChemRxiv*, 2024, doi: 10.26434/chemrxiv-2024-r5qsk.
- [53] J. Young, E. García-Díez, S. Garcia, and M. van der Spek, "The impact of binary water–CO₂ isotherm models on the optimal performance of sorbent-based direct air capture processes," *Energy & Environmental Science*, vol. 14, no. 10, pp. 5377-5394, 2021, doi: 10.1039/d1ee01272j.

- [54] M. J. Bos, T. Kreuger, S. R. A. Kersten, and D. W. F. Brilman, "Study on transport phenomena and intrinsic kinetics for CO₂ adsorption in solid amine sorbent," *Chemical Engineering Journal*, vol. 377, 2019, doi: 10.1016/j.cej.2018.11.072.
- [55] X. Hu, E. Mangano, D. Friedrich, H. Ahn, and S. Brandani, "Diffusion mechanism of CO₂ in 13X zeolite beads," *Adsorption*, vol. 20, no. 1, pp. 121-135, 2013, doi: 10.1007/s10450-013-9554-z.
- [56] Lanxess. "Product Information Lewatit VP OC 1065." <https://lanxess.com/en/Products-and-Brands/Products//LEWATIT--VP-OC-1065> (accessed 2024).
- [57] Purolite. "Purolite A110." <https://www.purolite.com/product-pdf/A110.pdf> (accessed 2023).
- [58] H. Azzan, A. K. Rajagopalan, A. L'Hermitte, R. Pini, and C. Petit, "Simultaneous Estimation of Gas Adsorption Equilibria and Kinetics of Individual Shaped Adsorbents," *Chem Mater*, vol. 34, no. 15, pp. 6671-6686, Aug 9 2022, doi: 10.1021/acs.chemmater.2c01567.